*Int. J. Electrochem. Sci.*, 15 **(2020)** 7459 – 7473, doi: 10.20964/2020.08.54

International Journal of
ELECTROCHEMICAL
SCIENCE
www.electrochemsci.org

# Electrochemical Performance Evaluation of Galvanostatically Deposited Co(OH)₂ on Few-Layered Graphene Electrodes

*V. Parra−Elizondo*[1, 2], *J.M. Baas−López*[2] *and D. Pacheco−Catalán*[2,*]

[1] Universidad Tecnológica Metropolitana, Calle 115 Circuito Colonias Sur No. 404, Santa Rosa, 97279 Mérida, Yucatán, México Tel :01(52) 999 940 6102
[2] Centro de Investigación Científica de Yucatán, A.C. Carretera Sierra Papacal−Chuburná Puerto Km 5, Sierra Papacal, 97302 Mérida, Yucatán; México Tel :01(52)9999428330
*E-mail: dpacheco@cicy.mx

*Received:* 9 March 2020 / *Accepted:* 11 May 2020 / *Published:* 10 July 2020

---

In this paper, an electrochemical performance evaluation of galvanostatically deposited $Co(OH)_2$ onto few-layered graphene (FLG) is presented. The electrochemical evaluation was carried out in a two-electrode symmetric cell arrangement. Electrodes were synthesized by combining FLG made through simple instrumentation atmospheric pressure–chemical vapor deposition (AP−CVD) process onto Cu foil substrates, and galvanostatically deposited Co by chronopotentiometry deposition. Faradaic contributions of as-deposited $Co(OH)_2$ increase the areal capacity of the electrochemical cells (EC) with an areal capacity of 0.72 μA h $cm^{-2}$, in comparison with the FLG EC with an areal capacity of 0.04 μA h $cm^{-2}$ at 4 mA $cm^{-2}$. Along with the areal capacity enhancement, specific energy, as the galvanostatic charge/discharge evaluation tells, showed a boost from 0.434 to 7.79 mW h $g^{-1}$ evaluated at 4 mA $cm^{-2}$, when the EC is galvanostatically deposited with Co. In terms of specific power, both EC presents similar values around 335 mW $g^{-1}$. These results offer some insight into the electrochemical complexation of carbonaceous supports obtained from the bottom-up synthesis approach and how they can be tuned to increase the electrochemical storage capabilities of the materials.

---

**Keywords:** AP−CVD; few-layered graphene; galvanostatically deposited $Co(OH)_2$; electrochemical performance; energy storage

## 1. INTRODUCTION

The current energy consumption foresees scenarios where a total integration of renewable energy sources is demanded. Based on the energy gap enclosure within the actual renewable energy scenario and the fossil fuel diminishment and greenhouse emissions growths, optimal energy management is needed [1]. Along with the issue of fulfilling the energy requirements of actual scenarios, renewable sources must address the intermittency in the generation and distributions of energy from renewable sources, such as in eolic and photovoltaic systems [2]. Currently, through the implementation of energy storage systems such as batteries and electrochemical capacitors, this problem is being addressed. At present, there are several mechanisms in which energy can be stored, e.g., through mechanical [3], thermal [4], and electrochemical systems [5]. Electrochemical systems are mainly represented by electrochemical capacitors and batteries, which are also the most versatile technologies due to their portability and tunable performance. Electrochemical capacitors offer an advantage in terms of life cycling and low maintenance of their batteries, along with high specific power output given by the storage mechanism allowing rapid charge/discharge cycles [6]. Carbon materials have represented the building block for electrochemical capacitors in the past twenty years, since nanometer-scale carbon-based materials have been introduced and developed, such as single-walled carbon nanotubes reported by Ijima in 1991 [7], graphene, and the remarkable theoretic properties reported by Novoselov in 2004 [8]. This variety of types of carbon-based materials exists thanks to the different hybridizations of atoms, generating materials with different mechanical and physicochemical properties. Within the sp2 carbon allotrope family, graphene is currently one of the most booming materials in the research and development of applications in the last ten years [9]. The potential in the development of graphene relies on the different routes through which it can be obtained via chemical and physical processes offering a variety of graphene-derived materials depending on the synthesis route used. Among the different routes, bottom-up route synthesis offers simple instrumentation with variables over the external factors in the synthesis, such as temperature and pressure in the system [10]. Chemical vapor deposition (CVD) is the most common synthesis process to generate graphene from the bottom-up approach methodologies. The formation of the $sp_2$ carbon matrix occurs via the adsorption of the carbon atoms at high temperatures (1000 ºC). The adsorption takes place in the surface of the transition metal substrate that serves as a template, and mechanical support. In the synthesis, a series of gases interact for the formation of the carbonaceous matrix material, gases such as carbon precursor, and catalyst gas, and carrier gas participates in the CVD process [11]. CVD can be operated in a different range of pressures; since ultra-high vacuum and vacuum represent a major instrumentation, this work aims to present a synthesis procedure where the instrumentation is simplified by working at atmospheric pressure. This type of methodology is known as atmospheric pressure–chemical vapor deposition (AP–CVD) and requires no vacuum instrumentation, turning synthesis into a more scalable scenario.

Among the various energy density enhancers available, metal hydroxides and oxides improve the capacity of the devices. The primary feature of these hydroxide and metal oxide types of materials resides in the combined mechanism in which the energy transfer increases via faradic contributions by redox reactions, intercalation of the ions on its matrix, and the adsorption-desorption process. The sum of all these contributions plays an essential role in the overall charge mechanism [12]. Promoting electron transfer increases the specific energy in the storage process of the electrochemical storage devices [13]. In the literature, $Co(OH)_2$ has been reported as a material with a well-known electrochemical activity [14]. $Co(OH)_2$ can be obtained via different types of synthesis routes, such as chemical approaches [15-16] and electrochemical routes [17], using pulse current methods [18]. Electrochemical deposition routes offer a controllable and localized synthesis approach since the growth of the material can be directed by polarization orientation, resulting in a selective reduction via electrochemical cell configuration.

**Table 1.** Different synthesis approaches on similar hybrid electrodes literature review.

| **$Co(OH)_2$synthesis** | **Carbonaceous support** | **ElectrodePreparation** | **Electrochemical evaluation** | **Energy storage *transformed** | **Ref** |
|---|---|---|---|---|---|
| Electrosynthesis Chronoamperometry (-1.0 V, 2 h) | Graphene nanosheet (Enanotech Industry) | Slurry cast on a mesh<br>Mass ratio (100:15:10)<br>active material: conductivity enhancer: binder<br>Area: 2 $cm^2$ | Half cell configuration<br>Potential window -0.1- 0.4 V vs. Ag/AgCl<br>charge density 2 mA $cm^{-2}$<br>1M of KOH as electrolyte | 2.6 μA h $cm^{-2}$ | [19] |
| Hydrothermal synthesis | 3D graphene by AP-CVD on Ni foam | Binder free hydrothermal deposition<br>Area: 2 $cm^2$<br>Mass of $Co(OH)^2$: 0.15 mg | Half cell configuration<br>Potential window -0.15 - 0.45 V vs. Hg/HgO<br>charge density 0.5 mA $g^{-1}$<br>6M of KOH as electrolyte | 0.24 μA h $cm^{-2}$ | [20] |
| Hydrothermal precipitated and ultrasonicated exfoliated | Few-Layer Graphene of thermally expanded graphite | Mechanically mixture of powder precursor<br>Total mass: 16 mg | Two electrode cell configuration<br>Potential window -0.1-0.4V vs. Ag/AgCl<br>charge density 0.5 A $g^{-1}$<br>1 M of KOH as electrolyte | 27.7 μA h g | [16] |
| Electrosynthesis Chronoamperometry (-0.9 V, at room temperature) | Carbon nanotubes by CVD | Asymmetric ensemble<br>$Co(OH)_2$ on Ni foam<br>CNT growth by CVD on Ni foam<br>Area:3 $cm^2$ | Two electrode cell asymmetric configuration<br>Potential window -0.1 -0.5 V vs. SCE<br>charge density 0.15 A $g^{-1}$<br>2 M of KOH as electrolyte | 8.5 μA h $cm^{-2}$ | [21] |
| Chemical precipitation | Reduced graphite oxide by Hummer method | Slurry cast on Ni mesh<br>Mass ratio | Half cell configuration<br>Potential window | 11.8 μA h $cm^{-2}$ | [22] |

| | | | | | |
|---|---|---|---|---|---|
| | | (80:15:5)<br>Area: 1 cm$^2$ | -0.1 -0.4V vs. Ag/AgCl<br>Charge density 1 A g$^{-1}$<br>2 M of KOH as electrolyte | | |
| Hydrothermally precipitated at 180 °Cfor 12 h | Chemical exfoliated graphite sheets by Hummer method | Slurry cast on Ni mesh<br>Mass ratio (85:10:5)<br>Area: 1 cm$^2$ | Half cell configuration<br>Potential window -0.05- 0.45 V vs. SCE<br>charge density 0.1 A g$^{-1}$<br>6 M of KOH as electrolyte | 123.0 μA h | [23] |
| Chemical reduction by hexamethylenetetramine | Reduced graphite oxide by Hummer method | Slurry cast on Ni mesh<br>Mass ratio (85:10:5)<br>Total mass: 2.98 mg | Half cell configuration<br>Potential window -0.1-0.4 V vs. SCE<br>charge density 0.5 A g$^{-1}$<br>1 M of KOH as electrolyte | 5.7 μA h | [24] |
| Chemical microemulsion and thermally annealed under air at 550 °C | Graphite oxide nanosheets chemically exfoliated by Hummer method | A solvent mixture of precursors<br>Total mass: 4.6-4.9 mg | Half cell configuration<br>potential window -0.2 - 0.6 V vs. Ag/AgCl<br>scan rate 5 mV s$^{-1}$<br>2 M of KOH as electrolyte | 11.46 μA h | [25] |

* To compare the values from the literature, the capacitance data was converted into capacity. The conversion was made to multiply by a fixed factor in which the area and electrode mass were accounted, to transform the given units, the reported capacitance was multiple by ($W$/3600 $s$), and the resulting value was normalized with the given area or mass in the reference, where $W$ is the absolute value of the electrochemical potential window evaluated and $s$ seconds.

Table 1 summarizes recent literature research on similar hybrid electrodes from the base materials. Overall, the majority of reviewed studies focus on the slurry mixture approach used as the base of the electrode construction, along with the abundant use of reduced graphite oxide carbonaceous support. Meanwhile, in the $Co(OH)_2$ synthesis, a few studies use electrochemical synthesis as the bottom-up type of methodology, with the constant voltage set up. It is worth mentioning that few studies analyze the full cell approach in the electrochemical cell configuration. This paper presents simple instrumentation for an AP−CVD growth of carbonaceous supports to serve as the substrate for a galvanostatically deposited faradic $Co(OH)_2$, along with an electrochemical performance evaluation of the coupled material as electrodes in a thin layer electrochemical cell.

## 2. EXPERIMENTAL

### *2.1. Synthesis of graphene as carbonaceous support by CVD.*

The bottom−up synthesis approach for carbonaceous graphene supports was carried out via AP−CVD. A Lindberg Blue M Thermo Scientific tubular furnace was used for the deposition process. The synthesis was carried out in a quartz tube with a length of 1.2 m and an inner diameter of 2.54 cm; inside the tube, a quartz tray with dimensions of 7 cm long and 2 cm wide was inserted in the midsection and supported a Cu foil substrate (25 µm thickness and 99.98 % purity from Alfa Aesar). In order to remove impurities and oil residues, Cu foils were cleaned through a series of rinses of de-ionized water, then in isopropyl alcohol and acetone. Additionally, electropolishing was carried out in 80% $H_3PO_4$. The experimental conditions for the CVD process are as follows. The metal substrates were thermally annealed for one hour at a temperature of 1000 ºC under a gas mixture flow of 300 standard cubic centimeters (sccm) of Ar and 100 sccm of $H_2$; after the annealing process, $CH_4$ gas flow was introduced as a carbon precursor in the reaction tube with a 20 sccm flow for an hour. After the deposition precursor feed time was over, the $H_2$ flow was turned off for the cooling process under a 600 sccm Ar flow for three hours.

### *2.2. Co electrodeposition onto carbonaceous deposited Cu foil.*

In order to couple Co into a carbonaceous matrix, electrodeposition was carried out via a galvanostatically reduction of $Co(OH)_2$ by $OH^-$ generation on the Cu/G electrode obtained through AP−CVD. Electrodeposition was carried out in a three-electrode cell in a Biologic VSP potentiostat in chronopotentiometry mode. The electrochemical deposits were made in a 0.1 M $Co(NO_3)_2$ solution at a temperature of 60 ° C. The current density applied was −1.19 mA $cm^{-2}$. The experimental configuration was as follows: A 13 mm diameter deposited Cu/G foil served as a working electrode (WE), as counter electrode stainless steel mesh was used in an area ratio of 4:1 compared with the WE. Furthermore, a saturated calomel electrode served as the reference electrode.

### *2.3. Sample preparation for characterization.*

Morphological and physicochemical techniques evaluated the galvanostatically as-deposited materials. The morphology was studied via scanning electron microscopy (SEM) with a JEOL JSM-7001F microscope; the samples were scraped and dissolved in a solution of ethanol in a vial flask and sonicated to disperse the materials, and then a droplet of the dispersion was collocated in the carbon tape in a sample holder of the microscope and then sputtered by Au particles. For the composition evaluation, samples were obtained using the powder of the as-deposited materials to analyze the X-Ray diffraction patterns (XRD). The analysis was carried out employing a Bruker D8 advance diffractometer, within a diffraction angle (2θ) range from 10 to 80° and a step measure of 2° $\mathrm{min}^{-1}$. The obtained diffraction pattern was compared with the analysis data.

### *2.4. Raman spectroscopy of few-layered graphene by AP−CVD*

In order to analyze the characteristics of CVD products, deposited Cu foils (Cu/G) were transferred onto a Si/$SiO_2$ wafer to carry out Raman spectroscopic evaluations with a Raman Renishaw inVia confocal microscope with a 532 nm laser wavelength. The transfer process was carried out via the formation of mechanical polymeric support over the carbonaceous deposit (Cu/G) through the spin coating technique. The mechanical support was made from a polymethyl methacrylate (PMMA) solution 4 % w/w. A total of 50 µL of the polymer solution was dropped in the center of the moving substrate; the system was left spinning for 60 seconds until the solvent was evaporated. The samples were dried in a vacuum oven at 60 °C for 12 hours, then chemical etching of the Cu substrate was carried out using a 30% v/v $FeCl_3$ bath for 30 minutes until the Cu substrate was etched. The resulting polymeric film was recovered from the bath etching bath and washed in a series of baths of de-ionized water. Finally, G/PMMA film was poured out in Si/$SiO_2$ wafer, where the polymeric film was dissolved with acetone, dried, and baked for three hours at 350 ºC to remove residual PMMA on the wafer substrate.

## 3. RESULTS AND DISCUSSION

### *3.2. Morphological analysis*

The morphological analysis of the as-deposited samples is shown in Fig. 1.

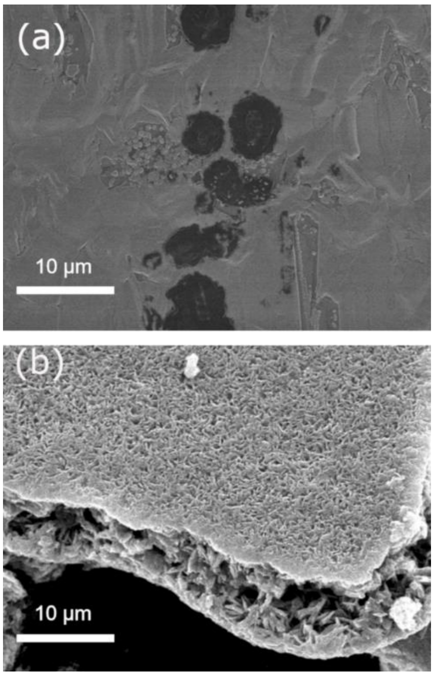

**Figure 1.** SEM micrographs of (a) as-deposited Cu−few-layered graphene (FLG) and (b) galvanostatically deposited $Co(OH)_2$.

The micrographs show the Cu/ few-layered graphene (FLG) deposited via AP-CVD (Fig. 1a) with carbonaceous domains with a 5 µm average size; the growth of the hexagonal islands agrees with a linear direction along the Cu grain substrate. Additionally, it can be seen as a smoother surface by the electropolished substrate. The Cu substrate presents well-defined grain borders, which may be desirable to carbon growth in the AP-CVD. As Yu *et al.* [26] indicate, these sites could act as nucleation centers. Meanwhile, in Fig. 1b, the electrocoupled $Co(OH)_2$ displays a sandwich structure in which laminar platelets have grown from the inside out of the structure, and the laminar platelets present major length grain domains up to 80 µm depth and 10 µm width; this platelet structure is typical of hydroxyl metal compounds [27].

### *3.2. Raman spectroscopy of few-layered graphene by AP−CVD*

The Raman spectra of the AP−CVD of Fig. 2 shows three distinctive zones along the spectrum. The first zone shows the D band located at 1350 $cm^{-1}$ and associated with delocalized sp2 hybridization atoms, which is also associated with the degree of defects in carbon lattice [28]. The second signal located at 1569 $cm^{-1}$ corresponds to the G band, also known as the graphitic trace of the deposit, and it is associated with the energy bonds of the $sp_2$ carbonaceous matrix [29]. Finally, the resonance 2D band is observed at 2683 $cm^{-1}$; this band is characteristic of graphene materials, position, and the width of the band, giving information about the number of graphene layers in the deposits and the ratios of the intensities I2D/IG signals. This relationship is used to calculate the number of graphitic layers of graphene [30].

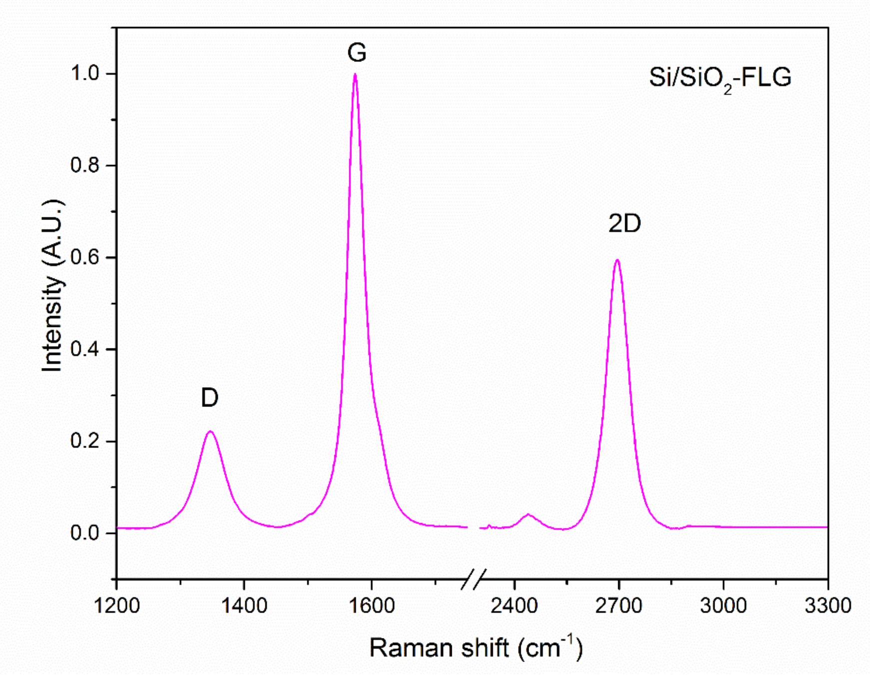

**Figure 2.** Raman spectra of the FLG sample.

The ratio between the two bands (2D and G) is used to quantify the number of layers of graphene [31]. The analysis in the literature shows that when the ratio is equal to or greater than two, the product obtained is single-layer graphene. As the ratio decreases, the number of graphene layers obtained increases, and identifying the graphene material from single to bi-layered up to few-layered graphene can be indexed. Another relationship between the ratios of the intensities in Raman spectroscopy is the ID/IG signals, which can determine the degree of defect in carbonaceous materials [32]. According to the analysis of the intensity ratios, the sample for the AP−CVD deposit has intensity ratios I2D/IG with a value of 0.499 and of 5.650 for the ID/IG ratio. The ratio can be attributed to a few-layered deposit with a low degree of disorder of the carbonaceous matrix. Experimental characterization by the position of resonance band 2D and intensity ratios of the AP−CVD product helps to identify the product as few-layered graphene (FLG), as the characterization by Dyakov *et al.* suggests [33].

The complementary intensity distribution map of the AP−CVD sample deposit can be seen in Fig. 3. The map shows a predominant G band area (Si/SiO$_2$-FLG) as the red intensity indicator suggesting the maximum relative intensity. This information gives some insight into the graphitized type of deposit made by the conditions of the AP-CVD in Section 2. D signals present a bigger distribution along the analyzed area than the resonance band 2D, suggesting that AP−CVD generates well-distributed FLG.

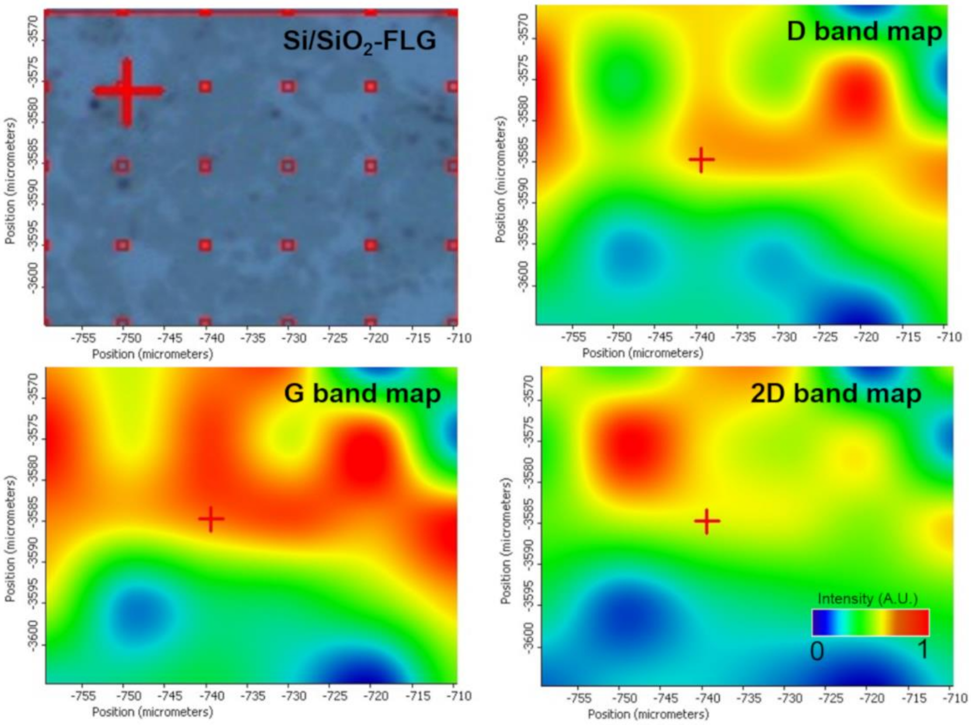

**Figure 3.** Raman distribution map of the relative intensities of D, G, and 2D signals in sample Si/SiO2−FLG.

Diffraction planes of the as-deposited Co(OH)$_2$ are shown in Fig. 4. The as-deposited powder shows diffraction plane signals for (003)(001), (100), (006), (011), and (012) located at 11.35, 19.12, 32.5, 33.05, 38.05, and 51.41°, respectively, which can be attributed to β-Co(OH)$_2$ according to crystallographic index JCPDS 74-1057 [34]. The presence in diffraction signals for the (003) and (006) planes located at 11.35 and 33.05º indicates the formation of mixed phases between rhombohedral α and β $Co(OH)_2$ [35]. The broadening of the small diffraction planes can be associated with the intercalated $NO_3^-$ in the sample.

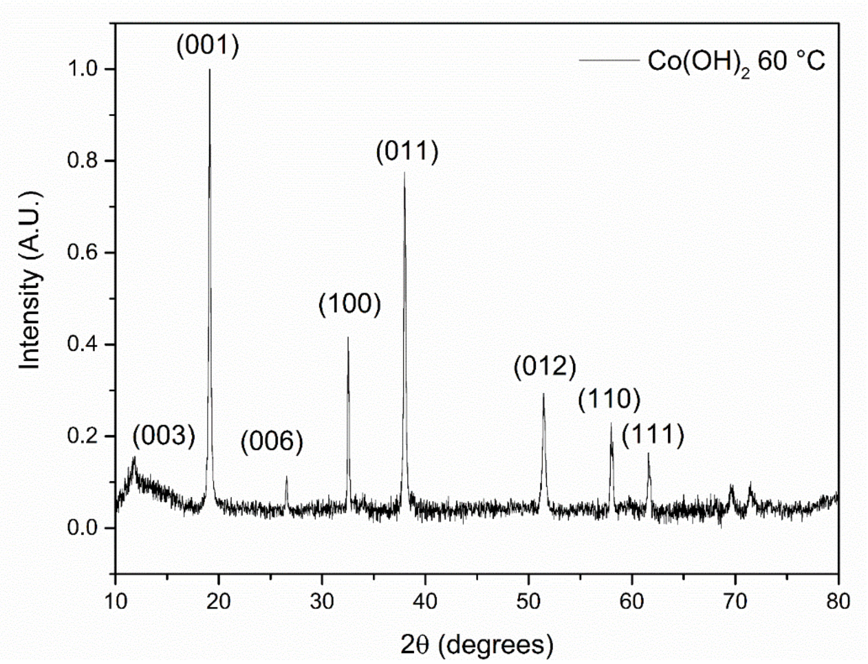

**Figure 4.** XRD diffractogram of as-deposited $Co(OH)_2$.

### *3.3. Electrochemical performance of composite material FLG/Co(OH)2*

Fig. 5a shows the voltammogram corresponding to the electrochemical cell (EC) assembled with two electrodes of the graphene FLG sample without cobalt electrodeposition, where the scanning rates evaluated are within a range of 2 to 50 mV $s^{-1}$. In the voltammogram, the signals of the oxidation and reduction process are observed after the 0.87 and 0.74 V potentials, respectively, for the oxidation and reduction process. These signals are characteristic of the oxidation and reduction of the copper support in the FLG EC [36]. The strong alkaline electrolyte favors this reaction, promoting the formation of an oxide layer, increasing the electrochemical activity present in the voltammogram (Fig. 5a) [37]. Likewise, the maximum current recorded was 4.6 µA $cm^{-2}$. It is essential to note the scan rate in which the phenomena of adsorption and desorption occur in the limits of cell potential, affecting the system response drastically as the cathodic current increases. Meanwhile, the FLG/$Co(OH)_2$ voltammogram presented in Fig. 5b shows the two oxidation and reduction peaks. The first pair is located at the potentials of 0.42 and 0.24 V, respectively, corresponding to the quasi-reversible oxidation-reduction of $Co(OH)_2$ onto CoOOH [38], while the second oxidation–reduction pair located at 0.9 and 0.5 V agrees with the Fig. 5a peaks. As mentioned before, these signals correspond to the oxidation of the copper oxide layer, and part of the recorded current is due to the contribution of the material in the electrode, suggesting that the Cu substrate in Cu/FLG is not entirely deposited via AP-CVD. Regarding the voltammetry analysis, it is observed that the electrochemical cell with $Co(OH)_2$ presents more significant electrochemical activity as the oxidation and reduction signals confirm, with a maximum 15.84 µA $cm^{-2}$ when it was evaluated at a speed of 10 mV $s^{-1}$.

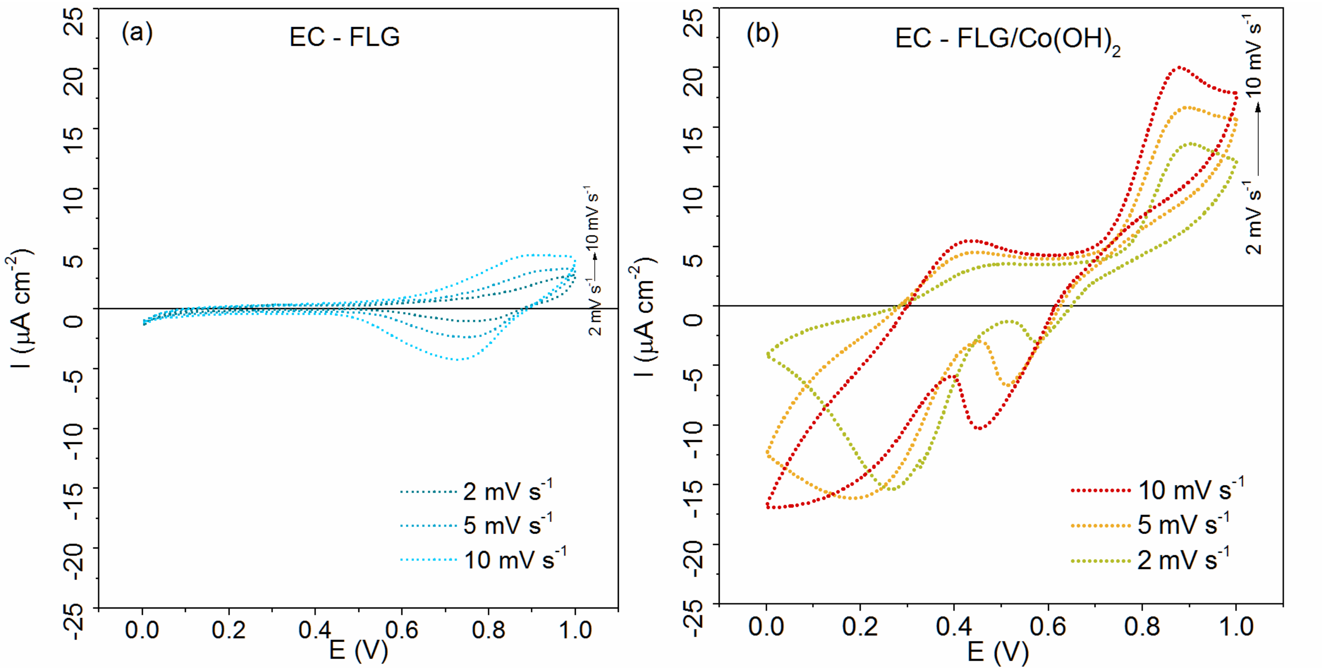

**Figure 5.** Comparative voltammograms of electrochemical cells of (a) as-deposited FLG and (b) coupled $Co(OH)_2$ onto FLG. In a potential window from 0 to 1 V in 2-electrode cell configuration, the electrochemical evaluation was carried out using 1 M KOH as an electrolyte.

Galvanostatic charge/discharge evaluation is presented in Fig. 6. The calculations were made using Equations (1) and (2):

$$Q_{Csc} = \frac{It_c}{m_E 3.6} \; (1).$$

$$Q_{Dsc} = \frac{It_d}{m_E 3.6} \; (2).$$

Where $Q_{Csc}$ and $Q_{Dsc}$ re the specific charge and discharge capacities, respectively; $I$ correspond to the charge density in which the EC was charged/discharged (from 1 to 10 mA $cm^{-2}$); $m_{EC,}$ corresponds to the mass of both electrodes in the cell; and 3.6 is a fixing factor to estimate the hourly rate of the capacity. In Fig. 6a, a comparison is presented, in which a sustainable difference can be observed in the areal capacity values. The FLG/$Co(OH)_2$ showed a maximum specific areal capacity of 41 µA h $cm^{-2}$ cm at the lowest charge density of 1 mA $cm^{-2}$, with a significant drop in the areal capacity as the charge increased, compared with the FLG EC, which presented a significantly lower capacity of 0.65 µA h $cm^{-2}$, with the difference of not presenting a significant drop in the charge/discharge densities.

The composite material FLG/$Co(OH)_2$ drop is associated with the faradic contribution of $Co(OH)_2$. The decrease is attributed to the charge transport in the oxidation-reduction of galvanostatically deposited $Co(OH)_2$ [39]. Coulombic efficiency analysis was calculated using the galvanostatic charge/discharge times obtained within the range of charge densities evaluated; the calculation was made recording the discharge time and the charge time. The ratio describes the efficiency in the charge/discharge process. The behavior along the interval presented in Fig. 6b shows the same tendency as the areal capacity plot for the FLG/$Co(OH)_2$ assembly, decreasing the efficiency up to 10% when the maximum current density 10mA $cm^{-2}$ was evaluated, unlike the FLG EC, where the efficiency remains nearly stable and above 90% across the charge/discharge currents evaluated.

Equivalent series resistance (ERS) in the EC is presented in Fig. 6c. Both assemblies presented values no greater than 0.8 Ω, which may suggest a proper assembly in the electrochemical cell (EC) array and a stable coupling of $Co(OH)_2$ in FLG/$Co(OH)_2$. Furthermore, the Ragone plot in Fig. 6d shows how the increase in charging density exhibits the attributes of each device, in which FLG presents a maximum value of specific energy of 1.23 mW h $g^{-1}$, decreasing to 0.17 Wh $kg^{-1}$ when the device was evaluated at the maximum charge density of 10 mA $cm^{-2}$, unlike FLG/$Co(OH)_2$ EC, which presented specific energy values of 44 Wh $kg^{-1}$ by the faradic contribution of $Co(OH)_2$. Regarding the specific power of the devices, the assemblies presented values of 845 and 904 mW $g^{-1}$ for the FLG and FLG/$Co(OH)_2$ capacity cells, respectively, which may suggest that the performance in the devices is limited by the charge density [40].

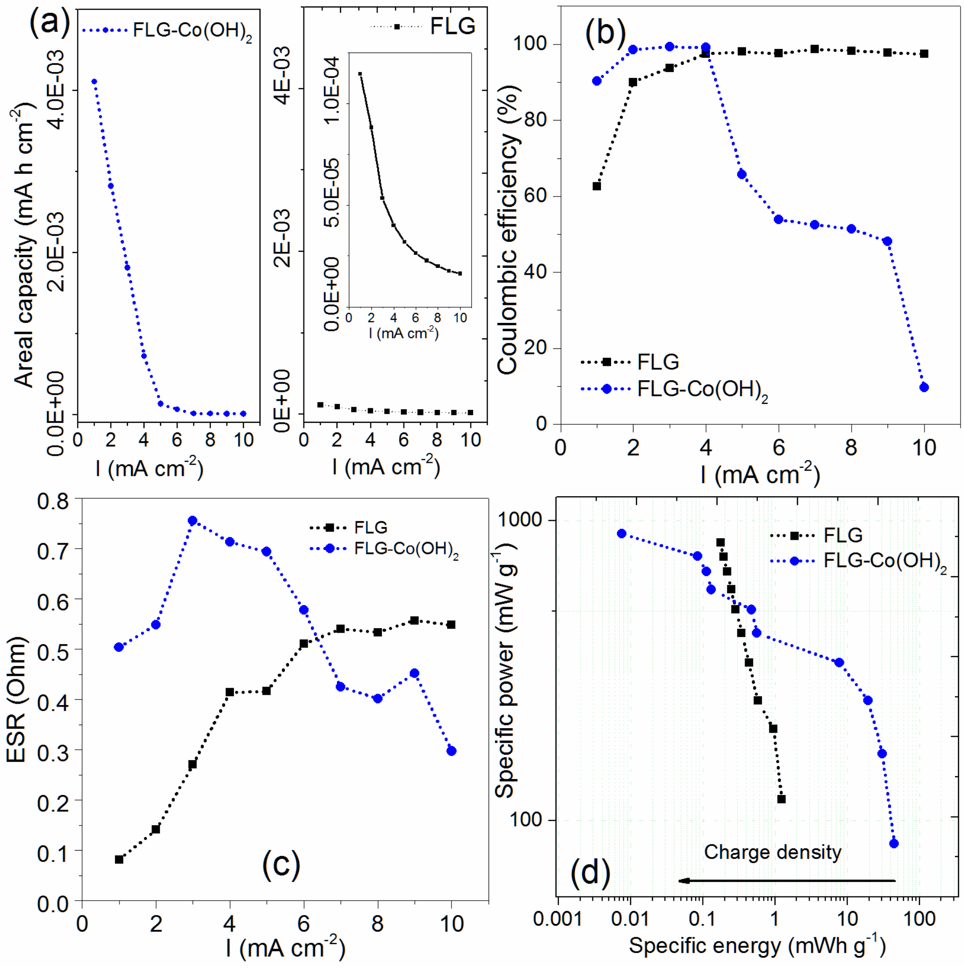

**Figure 6.** Galvanostatic charge/discharge analysis. (a) Areal capacity evaluation between FLG and FLG-$Co(OH)_2$ EC; (b) Coulombic efficiency analysis; (c) ESR of electrochemical cells (ECs) as a function of charge density; and (d) Ragone plot of FLG and FLG/$Co(OH)_2$ ECs.

Finally, it was observed through analysis via galvanostatic charge/discharge that the electrochemical cell based on FLG/Co(OH)$_2$ presented better electrochemical performance than the single support of FLG graphene due to the addition of galvanostatically deposited Co(OH)$_2$. However, the operation of the device was limited by the low charge density range in which the efficiency of the device was not compromised (4 mA cm$^{-2}$), unlike the FLG graphene EC, which operates stably at high charging densities which are higher than 4 mA cm$^{-2}$.

Potentiostatic electrochemical impedance analysis is presented in Fig. 7. Nyquist diagrams for the electrochemical cells based on FLG and FLG/Co(OH)$_2$ show a diagonal line pattern, and this distribution is attributed to the diffusion processes of the coupled materials via the alkaline media in which have been evaluated [41-42].

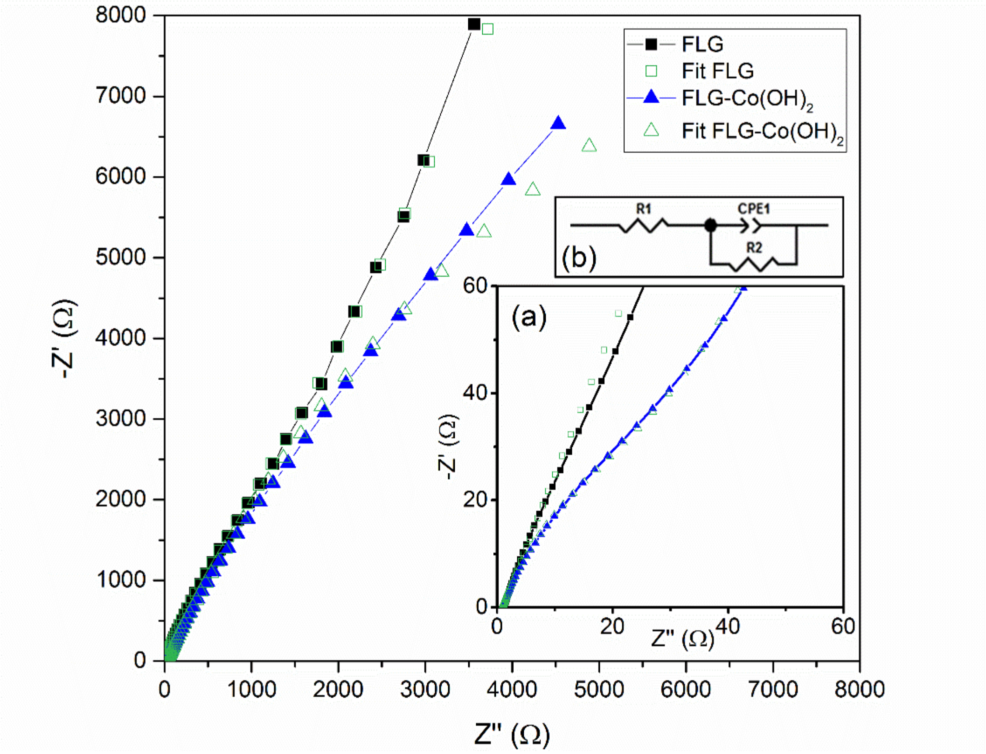

**Figure 7.** Nyquist diagrams of the FLG and FLG/Co-based ECs.

Likewise, the fitted experimental data was obtained through an equivalent circuit presented in Fig. 7b. The equivalent circuit was obtained utilizing the Zview2® software. The equivalent circuit components are assessed in Table 2. The equivalent circuit presents an equivalent series resistance R$_1$ element, followed by a constant phase element (CPE) connected in series, followed by a second resistor R$_2$ element in parallel. The resistance values are similar to those obtained through analysis by galvanostatic charge/discharge in Fig. 6c.

**Table 2.** Components of the equivalent circuit of the FLG and FLG/Co(OH)$_2$ ECs.

| EC | R$_1$ (Ω) | CPE$_1$-T | CPE$_1$-P | R$_2$ (Ω) | $\chi^2$ |
|---|---|---|---|---|---|
| **FLG** | 1.07E+00 | 1.13 E−4 | 0.766 | 5.15E+04 | 3.38 E−3 |
| **FLG-Co(OH)$_2$** | 6.46E-01 | 1.66 E−3 | 0.682 | 1.27E+05 | 1.19 E−2 |

For the resistance values, a difference between electrolyte resistance with values of 1.073 and 0.646 Ω is observed for the FLG and FLG/Co(OH)$_2$ thin layer EC, respectively, and the addition of Co(OH)$_2$ has a positive effect in the reduction of the resistance. Likewise, the constant phase element components for the phase angle (CPE-P) are more significant in the FLG EC with a value of 0.766, unlike in the 0.682 calculated for the phase angle of the FLG/Co(OH)$_2$ EC. Additionally, the resistance value R$_2$ associated with the resistance by charge transfer phenomena given at low frequencies is more than double that for the FLG/Co(OH)$_2$ EC, and a significant increment is given by the layer composition of Co(OH)$_2$. The adjustment coefficient $\chi^2$ agrees with the experimental data fitted by the equivalent circuit.

## 4. CONCLUSIONS

Chemical vapor deposition was achieved over copper substrates, resulting in the formation of a carbonaceous graphene (FLG) derivate. According to Raman spectroscopy analysis, a characteristic quotient of normalized intensity peak ratios for the signals I2D/IG registered a value of 0.499 and the ID/IG ratio with a value of 0.177, suggesting the formation of a few layers of graphene deposit via the presented synthesis methodology. The as-deposited material (FLG) served as mechanical support for the galvanostatically reduced Co(OH)$_2$, resulting in a hybrid electrode. The as-electrodeposited material (FLG/Co(OH)$_2$) showed a synergetic effect; the faradaic contributions of as-deposited Co(OH)$_2$ increased the areal capacity of the ECs with an areal capacity of 0.72 μA h cm$^{-2}$, in comparison with the FLG. EC with an areal capacity of 0.04 μA h cm$^{-2}$ at 4 mA cm$^{-2}$. Along with the areal capacity enhancement, specific energy increases, as the galvanostatic charge/discharge evaluation tells, from 0.434 to 7.79 mW h g$^{-1}$ evaluated at 4 mA cm$^{-2}$, when Co is localized reduced on the EC carbonaceous support. In terms of specific power, both EC's present values around 335 mW g$^{-1}$.

ACKNOWLEDGMENTS
This work was supported by the Consejo Nacional de Ciencia y Tecnología (Mexico) CB 2011−166356 project fund, CONACYT- SENER Sust. 254667 and student grant (362308), as well as Doctoral trainees, grant by CICY. The authors acknowledge the technical support for characterization from J. Dominguez-Maldonado, and E. Escobedo-Hernández (CICY) for the characterization of materials.

## References

1. H. Jiayi, J. Chuanwen, and X. Rong, *Renewable and Sustainable Energy Reviews*, 12 (2008) 2472-2483.
2. B. K. Sovacool, *Utilities Policy*, 17 (2009) 288-296.

3. A. Evans, V. Strezov, and T. J. Evans, *Renewable and Sustainable Energy Reviews*, 16 (2012) 4141-4147.
4. S. Kuravi, J. Trahan, D. Y. Goswami, M. M. Rahman, and E. K. Stefanakos, *Progress in Energy and Combustion Science*, 39 (2013) 285-319.
5. D. Pacheco, M. Smith , and E. Morales, *International Journal of Electrochemical Science*, 6(2011) 78-90.
6. L. L. Zhang and X. Zhao, *Chemical Society Reviews*, 38 (2009) 2520-2531.
7. S. Ijima, *Nature*, 354 (1991 ) 56.
8. A. K. a. N. Geim, K. S., *Nature Materials*, 6 ( 2007) 183–191.
9. A. K. Geim, *Science*, 324 (2009) 1530-1534.
10. W. Choi, I. Lahiri, R. Seelaboyina, and Y. S. Kang, *Critical Reviews in Solid State and Materials Sciences*, 35 (2010) 52-71.
11. I. A. Kostogrud, K. V. Trusov, and D. V. Smovzh, *Advanced Materials Interfaces*, 3 (2016) 1500823.
12. B. E. Conway and W. G. Pell, *Journal of Solid State Electrochemistry*, 7 (2003) 637-644.
13. Z. Lu, Z. Chang, W. Zhu, and X. Sun, *Chemical Communications*, 47 (2011) 9651-9653.
14. C. Chen, M. Cho, and Y. Lee, *Journal of Materials Science*, 50 (2015) 6491-6497.
15. J. T. Sampanthar and H. C. Zeng, *Journal of the American Chemical Society*, 124 (2002) 6668-6675.
16. J. P. Cheng, L. Liu, K. Y. Ma, X. Wang, Q. Q. Li, J. S. Wu, and F. Liu, *Journal of Colloid and Interface Science*, 486 (2017) 344-350.
17. J. T. Mehrabad, M. Aghazadeh, M. G. Maragheh, M. R. Ganjali, and P. Norouzi, *Materials Letters*, 184 (2016) 223-226.
18. M. Aghazadeh, S. Dalvand, and M. Hosseinifard, *Ceramics International*, 40 (2014) 3485-3493.
19. E. M. Jin, H. J. Lee, H.-B. Jun, and S. M. Jeong, *Korean Journal of Chemical Engineering*, 34 (2017) 885-891.
20. T. Yin, W. Zhang, Y. Yin, Y. Yan, K. Zhan, J. Yang, and B. Zhao, *Journal of Materials Science: Materials in Electronics*, 28 (2017) 7884-7891.
21. T. Peng, H. Wang, H. Yi, Y. Jing, P. Sun, and X. Wang, *Electrochimica Acta*, 176 (2015) 77-85.
22. Z. Li, J. Wang, L. Niu, J. Sun, P. Gong, W. Hong, L. Ma, and S. Yang, *Journal of Power Sources*, 245 (2014) 224-231.
23. G. Du, P. Liu, X. Yang, J. Zhang, X. Wang, and X. Sun, *RSC Advances*, 5 (2015) 38324-38329.
24. H. Wang, D. Wang, T. Deng, X. Zhang, C. Zhang, T. Qin, D. Cheng, Q. Zhao, Y. Xie, L. Shao, H. Zhang, W. Zhang, and W. Zheng, *Journal of Power Sources*, 399 (2018) 238-245.
25. J. Choi, T. Oh, M. Kim, J. Yang, and J. Kim, *Journal of Nanoscience and Nanotechnology*, 19 (2019) 1350-1359.
26. Q. Yu, L. A. Jauregui, W. Wu, R. Colby, J. Tian, Z. Su, H. Cao, Z. Liu, D. Pandey, and D. Wei, *Nature materials*, 10 (2011) 443.
27. Z. Liu, R. Ma, M. Osada, K. Takada, and T. Sasaki, *Journal of the American Chemical Society*, 127 (2005) 13869-13874.
28. L. Colombo, X. S. Li, B. Y. Han, C. Magnuson, W. W. Cai, Y. W. Zhu, and R. S. Ruoff, Graphene, Ge/Iii-V, and *Emerging Materials for Post-Cmos Applications* 2, 28 (2010) 109-114.
29. X. S. Li, C. W. Magnuson, A. Venugopal, J. H. An, J. W. Suk, B. Y. Han, M. Borysiak, W. W. Cai, A. Velamakanni, Y. W. Zhu, L. F. Fu, E. M. Vogel, E. Voelkl, L. Colombo, and R. S. Ruoff, *Nano Letters*, 10 (2010) 4328-4334.
30. A. C. Ferrari, J. C. Meyer, V. Scardaci, C. Casiraghi, M. Lazzeri, F. Mauri, S. Piscanec, D. Jiang, K. S. Novoselov, S. Roth, and A. K. Geim, *Physical Review Letters*, 97 (2006) 187401.
31. D. Yoon, H. Moon, Y.-W. Son, J. S. Choi, B. H. Park, Y. H. Cha, Y. D. Kim, and H. Cheong, *Physical Review* B, 80 (2009) 125422.

32. Q. H. Wang, Z. Jin, K. K. Kim, A. J. Hilmer, G. L. Paulus, C.-J. Shih, M.-H. Ham, J. D. Sanchez-Yamagishi, K. Watanabe, and T. Taniguchi, *Nature Chemistry*, 4 (2012) 724.
33. S. A. Dyakov, T. S. Perova, C. Q. Miao, Y. H. Xie, S. A. Cherevkov, and A. V. Baranov, *Journal of Raman Spectroscopy*, 44 (2013) 803-809.
34. L. Wang, J. Fu, Y. Zhang, X. Liu, Y. Yin, L. Dong, and S. Chen, *Progress in Natural Science: Materials International*, 26 (2016) 555-561.
35. Z. Liu, R. Ma, M. Osada, K. Takada, and T. Sasaki, *Journal of the American Chemical Society*, 127 (2005) 13869-13874.
36. G. Wang, J. Huang, S. Chen, Y. Gao, and D. Cao, *Journal of Power Sources*, 196 (2011) 5756-5760.
37. Y.-K. Hsu, Y.-C. Chen, and Y.-G. Lin, *Journal of Electroanalytical Chemistry*, 673 (2012) 43-47.
38. M. Ulaganathan, M. M. Maharjan, Q. Yan, V. Aravindan, and S. Madhavi, *Chemistry – An Asian Journal*, 12 (2017) 2127-2133.
39. A. Laheäär, P. Przygocki, Q. Abbas, and F. Béguin, *Electrochemistry Communications*, 60 (2015) 21-25.
40. R. Tian, S.-H. Park, P. J. King, G. Cunningham, J. Coelho, V. Nicolosi, and J. N. Coleman, *Nature Communications*, 10 (2019) 1933.
41. M.-J. Deng, P.-J. Ho, C.-Z. Song, S.-A. Chen, J.-F. Lee, J.-M. Chen, and K.-T. Lu, *Energy & Environmental Science*, 6 (2013) 2178-2185.
42. F. Xiao and Y. Xu, *Int. J. Electrochem. Sci.*, 7 (2012) 7440-7450.